

ENHANCING THE PERFORMANCE OF AN INTEGRATED NAVIGATION SYSTEM USING ON-LINE AND OFF-LINE CALIBRATION PROCEDURES

J. F. M. Lorga, F. Schubert, Q. P. Chu, and J. A. Mulder
Delft University of Technology
Delft, The Netherlands

Abstract

This paper analyzes and compares on-line and off-line calibration methods applied to an integrated navigation system. The influences in the global performances of using both methods separately or combined are shown. Ground data, collected in dynamic and static environments, is processed and incorporated using various Global Positioning System (GPS) observables to demonstrate the improved performances combining both calibration topologies.

1. Introduction

Terrestrial, maritime and aerial navigation applications respectively requiring centimeter, millimeter per second, and tenths of radian error level in position, velocity, and attitude have increased in the last few years and are no longer difficult to find. The challenging objective was to completely design and develop an integrated navigation system that achieves these performances.

The navigation system development started in the Fall 2002. The first results obtained by

simulations (see [1]) proved that it was possible to achieve the desired precisions. The design and implementation of the complete hardware and software is described in [2]. The first successful flight and ground tests are also presented in [2] and [3].

The present status of the navigation system is well illustrated by Fig. 1 in terms of software and hardware through the flowchart and pictures of the several components, respectively. The hardware main components are an Inertial Measurement Unit (IMU) composed of three fiber optic gyroscopes, three accelerometers and temperature sensors, a high-end Global

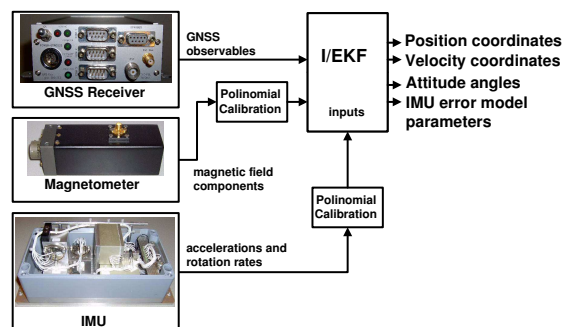


Fig. 1. Present status of the integrated navigation system.

Positioning System (GPS) receiver, and a three axis fluxgate magnetometer. A software application that uses an Extended Kalman Filter (EKF) or an Iterative EKF (IEKF) as the main integration filter was implemented. These types of filters were selected due to its superior performance in similar applications, as demonstrated in [4]. The flexible software application allows different combinations of unprocessed and processed GPS outputs to be used as measurements in the IEKF. Depending on the type of GPS observables used, two main integration topologies are possible: Loosely Coupled (LC) and Tightly Coupled (TC). The first topology uses the estimated position and velocity outputs of the GPS receiver, while the second can use C/A and P code pseudoranges, pseudorange rates (carrier Doppler), and carrier phase double differences of both L1 and L2 frequencies. The filter's GPS measurements are tightly complemented by the three axis raw outputs of the magnetometer.

The development of an integrated navigation system always includes calibration procedures of the sensors, in our case the accelerometers, gyroscopes, and magnetometer. The primary question is what type of calibration will improve more the performance of the integrated navigation system: the off-line calibration – usually in the polynomial form and commonly supplied by the components manufacturer; the on-line calibration – where the calibration parameters are states of the integration EKF; or the combination of both calibration types. Focusing on the calibration of inertial and magnetic sensors, only the LC topology was used because no GPS computations are done inside the integration filter. Therefore, the influences of the GPS algorithms are eliminated.

The remaining part of the paper is divided in four main sections. The first one describes the integration filter and its input equations. The second part discusses the off-line calibration of the inertial and magnetic sensors.

The third part describes the on-line calibration results using both static and dynamic data. The observability of the IMU error model parameters will also be addressed in this section. The conclusions section finalizes this paper.

2. The Integration Filter

The integration filter was implemented in a software application that facilitates the selection, just to mention some, of the integration topology, initial settings, measurements, and states. The states can be position and velocity coordinates, attitude angles, sensors temperatures, and the parameters from the sensors mathematical error models. The LC and TC integration topologies can use the same mathematical models for the IMU, which are used as inputs in the IEKF.

Typically, the differential equations of motion are written in the Navigation reference frame (North-East-Down, NED), see [5]. In this work all the equations of the system dynamics, also called kinematics equations, and the measurements equations were written in the Earth-Centered Earth-Fixed (ECEF) reference frame. The reasons for this choice are the convenience in writing the GPS measurements equations, in the TC integration topology, and to avoid computational problems sometimes experienced with the later conversion from NED to ECEF.

2.1. Input Equations

The inputs of the IEKF filter are obtained from the strap-down inertial sensors. Measurements from three accelerometers and three rate gyroscopes are used. These measurements can have errors originated by biases, scale factors, misalignments, non-linearities and measurement noises. The general mathematical error model used to represent the inertial sensors is similar for both accelerometers and rate gyroscopes. For the three specific forces measured by the ac-

celerometers the model is:

$$\begin{bmatrix} a_{xm} \\ a_{ym} \\ a_{zm} \end{bmatrix} = \begin{bmatrix} b_x \\ b_y \\ b_z \end{bmatrix} + \begin{bmatrix} w_x \\ w_y \\ w_z \end{bmatrix} + \begin{bmatrix} s_x & m_{xy} & m_{xz} \\ m_{yx} & s_y & m_{yz} \\ m_{zx} & m_{zy} & s_z \end{bmatrix} \begin{bmatrix} a_x \\ a_y \\ a_z \end{bmatrix}, \quad (1)$$

where a_{xm} , a_{ym} , and a_{zm} are the specific forces measured by the accelerometers in the body reference frame; a_x , a_y , and a_z are the real values of the specific forces also in body reference frame; s_x , s_y , and s_z are the scale factors; b_x , b_y , and b_z are the biases (the accelerometer bias derivative is equal to the drift); m_{xy} , m_{xz} , m_{yx} , m_{yz} , m_{zx} , and m_{zy} are the axis misalignments; and w_x , w_y , and w_z are the three body axes specific forces measurements noise. Since the accelerometers measurements are given in the body reference frame and all the other used equations were written in the ECEF reference frame, a coordinates transformation matrix from body to ECEF is necessary. The navigation system under development should be able to estimate besides the position, velocity, and attitude, the described parameters from the error models of the inertial sensors. The estimation of these parameters is obviously dependent in their observability which is discussed in Section 4.

3. Off-Line Calibration

The goal of the off-line calibration is to find the coefficients of the polynomial that relates the raw output of the sensors – measured in Volt – to the respective physical values. The next subsections describe the implemented off-line calibration procedures to the inertial and magnetic sensors.

3.1. Inertial

The inertial off-line calibration was initiated by placing the inertial sensors in a temperature controlled environment and several consecutive temperature cycles ranging from -40°C

to $+40^\circ\text{C}$ were applied. The cycle repetitions were done to detect the temperature dependent hysteresis of the components. Fig. 2 shows the changes in the outputs of the Z axis accelerometer and r gyroscope with temperature variations. For the accelerometers and gyroscopes a third and first order polynomial were used, respectively, to model the temperature influences.

The second part of the inertial calibration was done by using a tilt table to determine the accelerometers calibration polynomial coefficients for accelerations inferior to the gravity. This test consists in changing the attitude of the IMU box between exactly known positions imposing different accelerations to the accelerometers. The attitude angles imposed to the IMU can be known with an accuracy of 0.25 arc minute .

The used error model for the X axis accelerometer is:

$$\begin{aligned} a_{x \text{ real}} = & C_0 + C_1 a_x + C_2 a_x^2 + C_3 a_x^3 + C_4 a_x^4 \\ & + C_5 a_y + C_6 a_y^2 + C_7 a_z + C_8 a_z^2 + \\ & C_9 a_x a_y + C_{10} a_x a_z + C_{11} a_y a_z, \end{aligned} \quad (2)$$

where a_i are the accelerometers output and the coefficients C_i are determined using the least-squares method. The models for the Y and Z axis accelerometers are similar. The residuals between the true and the calibrated output are

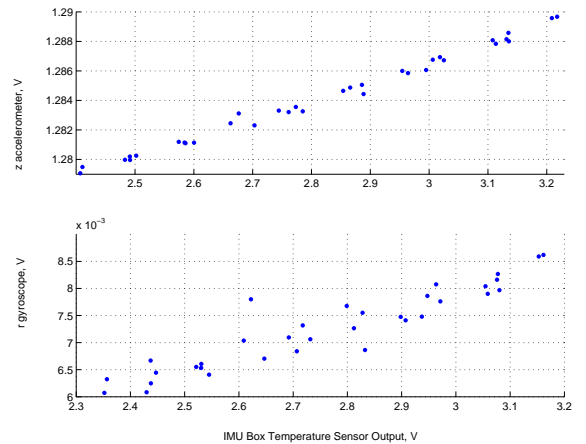


Fig. 2. Z accelerometer and r gyroscope temperature dependencies.

shown in Fig. 3. We can also see that our calibration outperforms the one supplied by the accelerometers manufacturer. This was expected because our calibration takes into account the axis misalignments and Analog-Digital Converter (ADC) card cross-coupling and change injection phenomena. These two phenomena are mainly caused by the ADC card miniaturization and the fact that a single ADC has to be multiplexed for the sixteen available channels.

The third calibration step of the inertial sensor was the calibration of the gyroscopes using a turn table. The used table can rotate around its vertical axis in both clockwise and counter-clockwise direction. The rotation speed can be adjusted from $0.01^\circ/s$ to $1200^\circ/s$.

The calibration procedure consisted in rotating the IMU around its three axes in both directions from $0^\circ/s$ to $300^\circ/s$. The collected data was processed and a polynomial calibration was applied to the three gyroscopes. The used p gyroscope the error model is:

$$p_{real} = C_0 + C_1p + C_2p^2 + C_3p^3 + C_5q + C_7r + C_9pq + C_{10}pr + C_{11}qr, \quad (3)$$

where p , q , and r are the gyroscopes outputs and coefficients C_i are determined using the least-squares method. The models for the q and r gyroscopes are similar. The residuals between

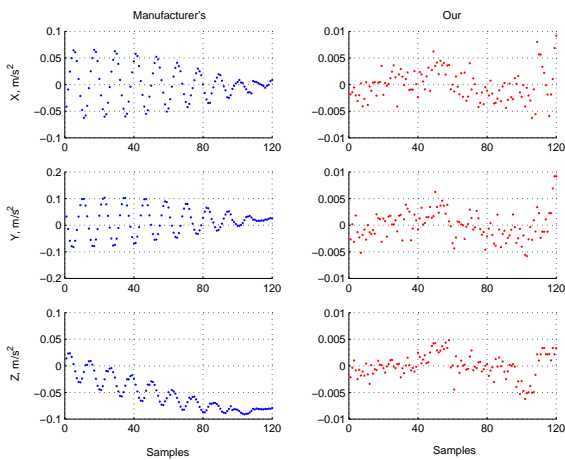


Fig. 3. Accelerometers calibration residuals.

the true and the calibrated output are shown in Fig. 4. We can also see that our calibration outperforms the simple one supplied by the gyroscopes manufacturer including only scale factors. This was expected because of misalignments estimation and ADC problems described previously.

3.2. Magnetic

Further improvements of the navigation system performance were achieved by applying the off-line magnetic calibration method described in [6]. This method does not require any external reference. Furthermore, unlike the usual calibration methods, it performs the calibration in the magnetic field domain and not in the heading domain. The results of the magnetic calibration are presented in Fig. 5. The system was rotated at constant a altitude. Therefore, the two horizontal components of the measured magnetic field, X and Y , have a sinusoidal behavior. When one of them is approximately zero, the other should point north and measure approximately 19018 nT , which is the horizontal intensity of the Earth's magnetic field at the tests location using the International Geomagnetic Reference Field model. The vertical axis Z and the norm of the magnetic field should have a constant value. The norm of the total magnetic field was

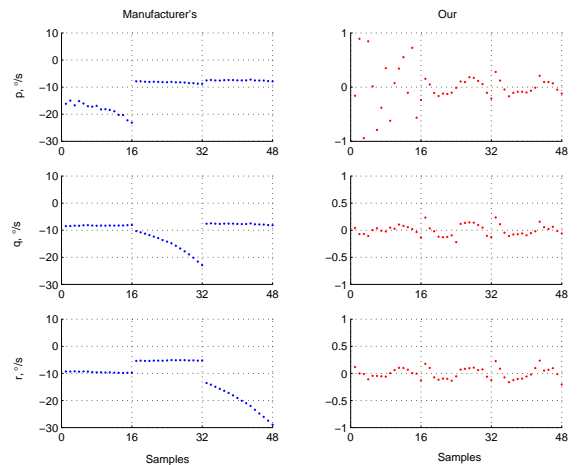


Fig. 4. Gyroscopes calibration residuals.

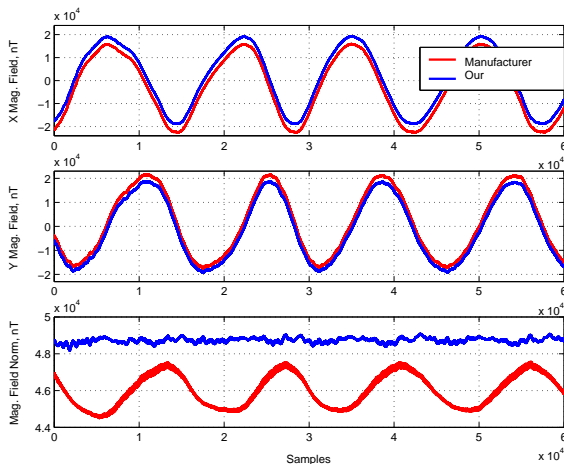


Fig. 5. Measured X , Y , and Earth magnetic field norm with and without our calibration.

approximately 48723 nT . The improvements achieved with the implemented calibration method are well visible in the top of the two plots of Fig. 5 showing the two horizontal axes. As expected, in these plots the sinusoid is centered around zero after the calibration. In the bottom plot, a constant magnetic field norm was achieved.

4. On-Line Calibration

In on-line calibration the inputs' error models parameters of the accelerometer and gyroscopes (see Eq. 1) are included as states in the EKF. Before all these parameters were introduced as states, an observability analysis was done.

4.1. States Observability

The summary of the observability analysis using the so-called Grammian matrix is presented in Table 1. This matrix is defined as:

$$G = \sum_{k=0}^N \Phi^T(k+1|0)H^T(k)H(k)\Phi(k+1|0) \quad (4)$$

where Φ is the system transition matrix and H the observation matrix. The system is completely observable if the matrix G is positive definite, or in other words, if all singular values are positive (non-zero) real values. The inclusion of the magnetometer was necessary to make observable the r gyroscope bias and the

heading angle under certain conditions. The misalignments only became observable when some maneuvers producing sufficient accelerations in all axes were performed. Furthermore, the mechanical misalignments of the system are constant, so once known they are always the same. Their inclusion as filter states would only add complexity to the filter and more computational power would be needed. Similar reasons led us also to exclude accelerometers and gyroscopes scale factors from the filter states. Additionally, as seen in the off-line calibration, a simple scale factor would not be sufficient for both type of sensors. Therefore, the polynomial coefficients from the inertial sensors error model (see Eq. 2) would also have to be added, raising new observability problems.

4.2. Static case

A LC filter was set up with 18 states: 3 position and 3 velocity coordinates, 3 attitude angles, 3 accelerometer and 3 gyroscopes biases, and 3 accelerometer temperatures. This configuration was used to process the data collected in the static and dynamic (see next subsection) environments.

The static test consisted in placing the navigation system with different attitudes. The selected roll and pitch angles were approximately 0° and 0° , -30° and 0° , and 0° and -30° , respectively. Their estimated values are presented in Fig. 6. As can be seen in all cases, the introduction of the off-line calibrations improved the quality of the final results. As seen in Fig. 7, the off-line calibrations not only influence position, velocity, and attitude estimation, but also the on-line calibration parameters, accelerometer and gyroscope

Table 1. Gyroscopes and accelerometers observable parameters from the input error models.

Is observable?	Gyroscopes	Accelerometers
Biases	Yes	Yes
Scale Factors	Yes	Yes
Misalignments	Not Always	Not Always

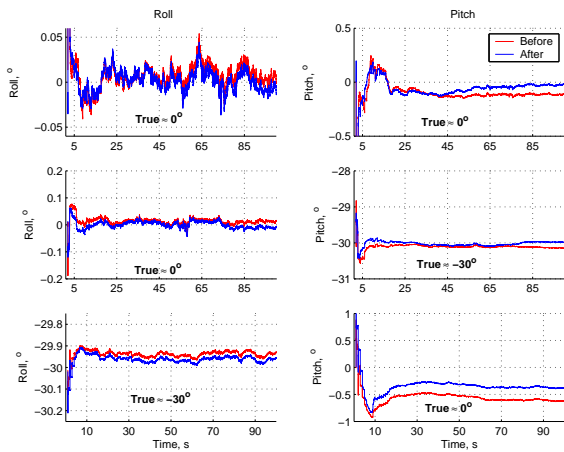


Fig. 6. Estimated roll and pitch in different situations.

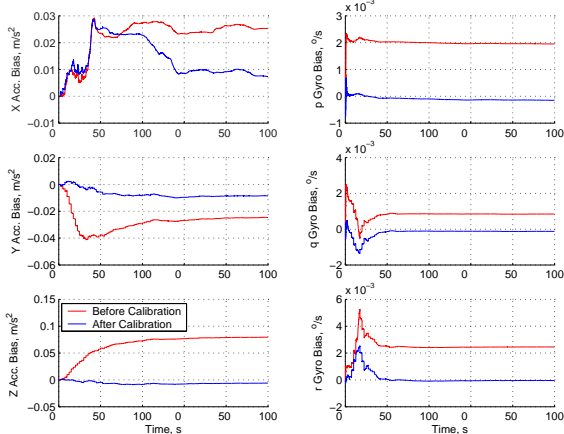


Fig. 7. Accelerometers and gyroscopes biases.

biases. The EKF includes in these biases the imprecisions and non-linearities of the used models, for instance, the Earth’s gravity and magnetic models. Therefore, it was expected that after the calibration these states had a smaller value, but still are different from zero.

4.3. Dynamic case

A set of ground tests were done to collect data in a dynamic environment. The GPS antenna was placed on the top of a van, the magnetometer on the tip of a 5 m aluminum boom sticking out of the van back, and the remaining components in the interior. These dynamic tests consisted in driving the van to an open field through a series of rectilinear

trajectories and perform circular maneuvers. The altitude changes were always inferior to 5m during the complete runs. The GPS board estimated heading angle – angle between body center line and true north – for one of the several completed runs can be seen in the top of Fig. 8.

The ground tests have the advantage of being done in a more controllable environment when compared to flight tests. Vertical and lateral body velocities are almost non existent, and the track angle – angle between ground speed and true north – is coincident with the van heading angle. The van velocity vector is coincident with the ground velocity vector. Therefore, the estimated heading angle of the LC filter can be compared with the track angle estimated by the GPS board, as it is also shown in Fig. 8. As expected, the moments the van is stopped the GPS board does not estimate correctly the heading angle. This can be seen in the top plot of Fig. 8 where the estimated GPS heading varied randomly between 0° and 360°.

The comparison of the GPS and LC estimated heading angles in the bottom plot of Fig. 8 show a 10° bias correction when the off-line magnetic calibration procedure is implemented.

The estimated pitch and roll attitude

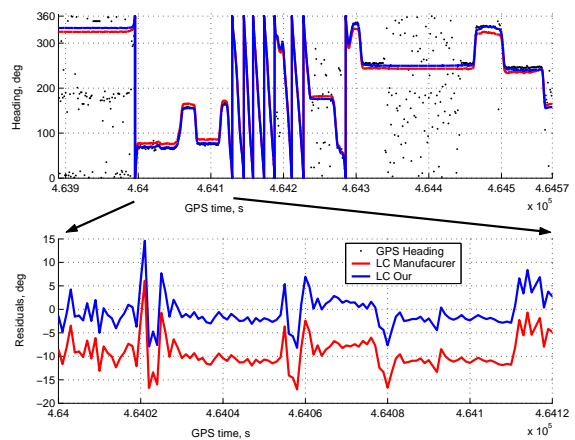


Fig. 8. GPS and LC using two different calibrations estimated van heading angle (top). The residuals between the GPS and LC heading for a shorter period (bottom).

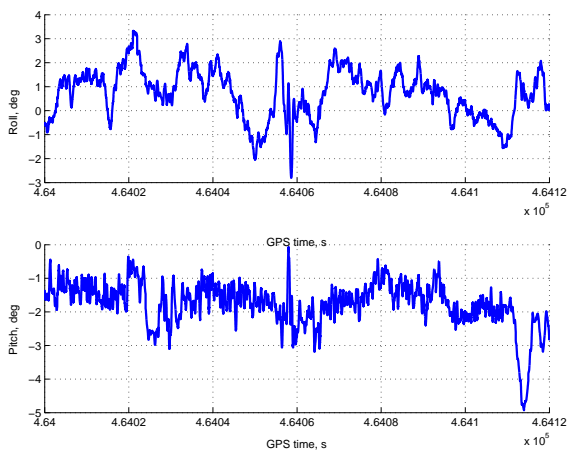


Fig. 9. EKF roll and pitch angle estimates.

angles, shown in Fig.9, should be approximately constant for all the run because it was performed in almost flat terrain with minor changes of altitude. No other source was available for comparison. Around 4.6406 s the break pedal was pushed hard, sudden changes of pitch and roll were registered. At the end of the run, the van was parked for some seconds in a small ramp, as can be seen by the increase in the pitch angle.

5. Conclusions

Enhances in overall performance of the integrated navigation system, through the employment of on-line and off-line calibration methods to the inertial and magnetic components were shown. The implemented off-line calibrations outperformed largely the ones supplied by the manufacturers because accounted for misalignments and ADC related problems. The biggest improvement was the correction of a 10° bias in the heading angle estimation due to poor magnetic calibration. Further improvements through off-line calibration will be achieved using the turn table and a metal arm, to extend the rotation radius, to excite the system with centrifugal accelerations superior to the gravity.

The best obtained configuration estimated the magnetic and inertial sensors biases, mis-

alignments and scale factors using off-line calibration methods, and an extra bias state in the EKF for each of the accelerometers and gyroscopes. This extra states improved the filter performance because imprecisions and non-linearities of the used models were 'looked' as a bias by the EKF.

Acknowledgments

The work presented and still under development is possible due to the financial and intellectual support of TNO - Defence, Security and Safety, The Hague, The Netherlands. The authors would also like to thank Kees van Woerkom for the help in the preparation of the ground experiments and system calibration.

References

- [1] Lorga J. F. M., Chu Q. P., and Mulder J. A. Tightly-coupled imu/gps carrier-phase navigation system. In *Proceedings of the Institute of Navigation 2003 National Technical Meeting*, pages 385–396, Anaheim, California, 22-24 January 2003. Institute of Navigation.
- [2] Lorga J. F. M., van Rossum W., van Halsema E., Chu Q. P., and Mulder J. A. The development of a sar dedicated navigation system: From scratch to the first test flight. In *PLANS 2004 - Position Location and Navigation Symposium Proceedings*, pages 249–258, Monterey, California, 26-29 April 2004. IEEE Aerospace and Electronic Systems Society.
- [3] Lorga J. F. M., Chu Q. P., van Rossum W., and Mulder J. A. Developing and testing a tightly coupled gps/imu navigation system. In *2nd ESA Workshop on Satellite Navigation User Equipment Technologies Navitec 2004 Workshop Proceedings*, Noordwijk, The Netherlands, 8-10 December 2004. European Space Agency - ESTEC.
- [4] Chu Q. P., Mulder J. A., and Van Woerkom P. T. L. M. Modified recursive maximum likelihood adaptive filter for nonlinear aircraft flight-path reconstruction. *Journal of Guidance, Control, and Dynamics*, 19(6):1285–1295, November-December 1996.
- [5] Mulder J.A., Chu Q.P., Sridha J.K. and Breeman J.H., and Laban M. Non-linear aircraft flight path reconstruction review and new advances. *Progress in Aerospace Sciences*, 35:673–726, 1999.
- [6] Elkaim G. H., Gebre-Egziabher D., Powell J. D., and Parkinson W. B. A non-linear, two-step estimation algorithm for calibrating solid-state strapdown magnetometers. In *8th St. Petersburg Conference on Navigation Systems (IEEE/AIAA)*, St. Petersburg, Russia, 27-31 May 2001.